

SPARSE LOCALIZATION OF BREAST TUMORS USING QUASI-TE POLARIZED ANTENNAS

Marija Nikolić Stevanović¹, Jelena Dinkić¹, Antonije Đorđević^{1,2},
Jasmin Musić³, Lorenzo Crocco⁴

¹University of Belgrade – School of Electrical Engineering, Belgrade, Serbia

²Serbian Academy of Sciences and Arts, Belgrade, Serbia

³WIPL-D d.o.o., Belgrade, Serbia

⁴Institute for the Electromagnetic Sensing of the Environment –
National Research Council, IREA-CNR, Naples, Italy

Abstract. *We develop a three-dimensional (3D) sparse algorithm for localization of breast tumors, using an antenna array and signal processing. Assuming that the prior-knowledge of the breast tissue distribution is available, we develop a model in which the trans-polarization is fully taken into account. By considering various array configurations, we also investigate the robustness of the algorithm to the inaccuracies in the assumed electromagnetic parameters of the breast.*

Key words: *breast imaging, compressive sensing, inverse scattering, microwave imaging*

1. INTRODUCTION

In the recent years, there has been a growing interest in microwave medical imaging [1], [2]. Compared to the conventional technologies, the main advantages of microwave imaging systems are their portability, low-cost, and non-ionizing radiation. The majority of clinical applications have focused on breast imaging, e.g., [2]–[5], but lately the efforts have been extended to other modalities such as bone [6] and brain imaging [7]–[9]. Numerous techniques have been proposed for this purpose. Some examples are the time-domain beamforming [5], the conjugate gradient approach [10]–[12], Gauss-Newton optimization [4], [13], etc.

Lately, compressive sensing techniques [14], [15] have been used for solving a number of microwave imaging problems [16]–[21]. Compressive sensing (sparse) imaging is known to yield clean and focused images with suppressed artifacts. Sparse imaging is particularly suitable for situations in which targets occupy only a small part of the observed domain. Typically, this is the case in differential microwave imaging, where

Received May 15, 2016; received in revised form September 15, 2016

Corresponding author: Marija Nikolić Stevanović

School of Electrical Engineering, Bulevar kralja Aleksandra 73, 11120 Belgrade, Serbia

(E-mail: mnikolic@etf.rs)

the goal is to locate small changes between consecutive measurements, rather than retrieving the permittivity of the whole investigated domain. Examples of differential microwave imaging apparatuses are the wearable breast-cancer detection system [22], [23] and the stroke-finder system [24].

Here, we consider the application of the compressive sensing for the three-dimensional (3D) breast-cancer localization. We assume that dipole-like antennas are placed parallel to circles encompassing the breast surface¹, which is analogous to the transverse electric (TE) polarization in the two dimensional (2D) geometry. This is in contrast to the usual approach in which the antennas are parallel to each other, as in the case of transverse magnetic polarization (TM). However, one must consider a full 3D model in which all field components are taken into account, unlike in the quasi-TM measurement configuration.

Assuming that variations of the tissue parameters (due to the possible tumor presence) between two measurements are small, it is possible to linearize the scattering equations. However, it is still necessary to compute 3D (dyadic) Green's functions, as well as the approximate field inside the breast. For this purpose, we assume to have a prior knowledge of the healthy breast tissue parameters. We also investigate the robustness of the algorithm against the errors in the tissue permittivity. By combining the obtained results in a particular way, we suppress false targets caused by the parameter ambiguity.

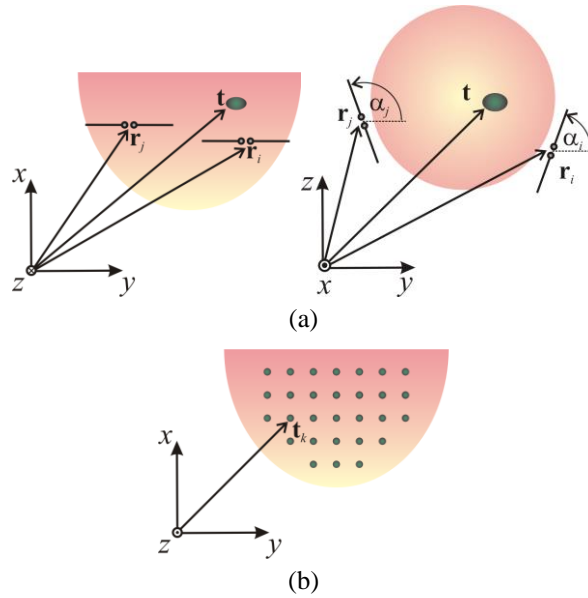


Fig. 1 (a) Measurement model and (b) sketch of 3D grid used in sparse processing

The organization of the paper is as follows. In the Section II, we describe the electromagnetic model. In Section III, we develop the sparse algorithm. In Section IV, we detail the inhomogeneous breast phantom that was used in simulations. Finally, in Section V, we provide some numerical results.

¹ In clinical examinations, the patient typically lies in prone position, with breasts pointing downwards, inside the imaging system. Hence, the field radiated by the array is horizontally polarized.

2. MEASUREMENT MODEL

We consider the measurement scenario depicted in Fig. 1(a). An unknown target or lesion (illustrated as an elliptic inclusion) is located inside the non-magnetic inhomogeneous breast tissue. To determine the location of the target, we use an antenna array placed around the breast in the vicinity of the skin. According to the coordinate system given in Fig. 1, the antennas are parallel to the yz plane, i.e., parallel to the chest wall. For simplicity, we show only two antennas: a transmitter, located at \mathbf{r}_i , and a receiver, located at \mathbf{r}_j . We define the scattered field as

$$\mathbf{E}_s(\mathbf{r}) = \mathbf{E}(\mathbf{r}) - \mathbf{E}_b(\mathbf{r}), \quad (1)$$

where $\mathbf{E}(\mathbf{r})$ and $\mathbf{E}_b(\mathbf{r})$ are the electric field vectors, measured at the field point \mathbf{r} , when the target is inside the breast and when there is no target (healthy breast), respectively. Using the volume equivalence principle [24], the scattered field may be expressed as

$$\mathbf{E}_s(\mathbf{r}) = \int_v \overline{\mathbf{G}}_b(\mathbf{r}, \mathbf{r}') \cdot \mathbf{J}_{\text{eq}}(\mathbf{r}') \, dV = \int_v \overline{\mathbf{G}}_b(\mathbf{r}, \mathbf{r}') \cdot j\omega(\varepsilon(\mathbf{r}') - \varepsilon_b(\mathbf{r}')) \mathbf{E}(\mathbf{r}') \, dV, \quad (2)$$

where \mathbf{r}' is the source position vector, $\overline{\mathbf{G}}_b(\mathbf{r}, \mathbf{r}')$ is the Dyadic background Green's function, $\mathbf{J}_{\text{eq}}(\mathbf{r}')$ is the equivalent current density vector, $\mathbf{E}(\mathbf{r}')$ is the total field inside the breast, ε_b is the permittivity of the healthy breast, ε is the permittivity of the target ($\varepsilon \neq \varepsilon_b$), and v is the breast volume. If the target is electrically small, (2) becomes

$$\mathbf{E}_s(\mathbf{r}) \approx j\omega(\varepsilon - \varepsilon_b(\mathbf{r}')) \overline{\mathbf{G}}_b(\mathbf{r}, \mathbf{t}) \mathbf{E}(\mathbf{t}) \Delta V, \quad (3)$$

where \mathbf{t} is the target position vector and ΔV is its volume. Supposing that the target is a weak scatterer, we have

$$\mathbf{E}_s(\mathbf{r}) \approx j\omega(\varepsilon - \varepsilon_b) \overline{\mathbf{G}}_b(\mathbf{r}, \mathbf{t}) \mathbf{E}_b(\mathbf{t}) \Delta V, \quad (4)$$

where $\mathbf{E}_b(\mathbf{t}) \approx \mathbf{E}(\mathbf{t})$ is the background electric field. We express the background field in terms of 3D Green's function as

$$\mathbf{E}_b(\mathbf{t}) = \int_{l_a} \overline{\mathbf{G}}_b(\mathbf{t}, \mathbf{l}) \cdot I(\mathbf{l}) d\mathbf{l}, \quad (5)$$

where \mathbf{l} is the source vector, I is the current of the transmitting antenna, and l_a is the antenna length. Assuming that the antennas are electrically short dipoles (without top loadings), the current distribution is approximately triangular, i.e., $I(l) = I_0(1 - l/h)$, $|l| \leq h$, where I_0 is the current at the port of the dipole, h is the length of the dipole arm, and l is the local coordinate. Using this approximation, (5) becomes

$$\mathbf{E}_b(\mathbf{t}) \approx \overline{\mathbf{G}}_b(\mathbf{t}, \mathbf{r}_i) \cdot \int_{l_a} I(\mathbf{l}) \, d\mathbf{l} = I_0 \overline{\mathbf{G}}_b(\mathbf{t}, \mathbf{r}_i) \cdot \mathbf{h}_i, \quad \|\mathbf{h}_i\| = h, \quad (6)$$

where \mathbf{r}_i is the location of the transmitter and \mathbf{h}_i is the vector in the direction of the current, parallel to the dipole axis. Hence, the scattered field at the receiver is

$$\mathbf{E}_s(\mathbf{r}_j, \mathbf{r}_i) \approx j\omega(\varepsilon - \varepsilon_b) \overline{\mathbf{G}}_b(\mathbf{r}_j, \mathbf{t}) \overline{\mathbf{G}}_b(\mathbf{t}, \mathbf{r}_i) \cdot \mathbf{h}_i I_0 \Delta V, \quad (7)$$

where \mathbf{r}_j is the location of the j th receiver. Due to the reciprocity, i.e., $\overline{\mathbf{G}}_b(\mathbf{r}, \mathbf{t}) = \overline{\mathbf{G}}_b(\mathbf{t}, \mathbf{r})^T$,

$$\mathbf{E}_s(\mathbf{r}_j, \mathbf{r}_i) \approx j\omega(\varepsilon - \varepsilon_b)(\overline{\mathbf{G}}_b(\mathbf{t}, \mathbf{r}_j))^T \overline{\mathbf{G}}_b(\mathbf{t}, \mathbf{r}_i) \cdot \mathbf{h} I_0 \Delta V. \quad (8)$$

In our case, both the transmitting and receiving antennas are parallel to the yz plane. Hence, the scattered field at the location of the j th antenna, when the i th antenna is transmitting, is

$$\mathbf{E}_s(\mathbf{r}_j, \mathbf{r}_i) \approx K \begin{bmatrix} G_{xx}(\mathbf{t}, \mathbf{r}_j) & G_{yx}(\mathbf{t}, \mathbf{r}_j) & G_{zx}(\mathbf{t}, \mathbf{r}_j) \\ G_{xy}(\mathbf{t}, \mathbf{r}_j) & G_{yy}(\mathbf{t}, \mathbf{r}_j) & G_{zy}(\mathbf{t}, \mathbf{r}_j) \\ G_{xz}(\mathbf{t}, \mathbf{r}_j) & G_{yz}(\mathbf{t}, \mathbf{r}_j) & G_{zz}(\mathbf{t}, \mathbf{r}_j) \end{bmatrix} \begin{bmatrix} G_{xx}(\mathbf{t}, \mathbf{r}_i) & G_{xy}(\mathbf{t}, \mathbf{r}_i) & G_{xz}(\mathbf{t}, \mathbf{r}_i) \\ G_{yx}(\mathbf{t}, \mathbf{r}_i) & G_{yy}(\mathbf{t}, \mathbf{r}_i) & G_{yz}(\mathbf{t}, \mathbf{r}_i) \\ G_{zx}(\mathbf{t}, \mathbf{r}_i) & G_{zy}(\mathbf{t}, \mathbf{r}_i) & G_{zz}(\mathbf{t}, \mathbf{r}_i) \end{bmatrix} \begin{bmatrix} 0 \\ \cos \alpha_i \\ \sin \alpha_i \end{bmatrix}, \quad (9)$$

where $K = j\omega(\varepsilon - \varepsilon_b)I_0 h \Delta V$, $\mathbf{h}_i = h(\cos \alpha_i \mathbf{i}_y + \sin \alpha_i \mathbf{i}_z)$, and α_i is the angle defined in Fig. 1(a). In the expanded form, (9) is

$$\begin{bmatrix} E_{s,y}(\mathbf{r}_j, \mathbf{r}_i) \\ E_{s,z}(\mathbf{r}_j, \mathbf{r}_i) \end{bmatrix} = K \begin{bmatrix} g_{11} & g_{12} \\ g_{21} & g_{22} \end{bmatrix} \begin{bmatrix} \cos \alpha_i \\ \sin \alpha_i \end{bmatrix}, \quad (10)$$

$$g_{11} = (G_{xy}(\mathbf{t}, \mathbf{r}_j)G_{xy}(\mathbf{t}, \mathbf{r}_i) + G_{yy}(\mathbf{t}, \mathbf{r}_j)G_{yy}(\mathbf{t}, \mathbf{r}_i) + G_{zy}(\mathbf{t}, \mathbf{r}_j)G_{zy}(\mathbf{t}, \mathbf{r}_i)), \quad (11)$$

$$g_{12} = (G_{xy}(\mathbf{t}, \mathbf{r}_j)G_{xz}(\mathbf{t}, \mathbf{r}_i) + G_{yy}(\mathbf{t}, \mathbf{r}_j)G_{yz}(\mathbf{t}, \mathbf{r}_i) + G_{zy}(\mathbf{t}, \mathbf{r}_j)G_{zz}(\mathbf{t}, \mathbf{r}_i)), \quad (12)$$

$$g_{21} = (G_{xz}(\mathbf{t}, \mathbf{r}_j)G_{xy}(\mathbf{t}, \mathbf{r}_i) + G_{yz}(\mathbf{t}, \mathbf{r}_j)G_{yy}(\mathbf{t}, \mathbf{r}_i) + G_{zz}(\mathbf{t}, \mathbf{r}_j)G_{zy}(\mathbf{t}, \mathbf{r}_i)), \quad (13)$$

$$g_{22} = (G_{xz}(\mathbf{t}, \mathbf{r}_j)G_{xz}(\mathbf{t}, \mathbf{r}_i) + G_{yz}(\mathbf{t}, \mathbf{r}_j)G_{yz}(\mathbf{t}, \mathbf{r}_i) + G_{zz}(\mathbf{t}, \mathbf{r}_j)G_{zz}(\mathbf{t}, \mathbf{r}_i)). \quad (14)$$

Finally, the induced voltage at the j th antenna, due to the scattering from the target, is

$$V(\mathbf{r}_j, \mathbf{r}_i) = -\mathbf{E}_s \cdot \mathbf{h}_j, \quad \mathbf{h}_j = h(\cos \alpha_j \mathbf{i}_y + \sin \alpha_j \mathbf{i}_z), \quad (15)$$

where α_j is the angle defined in Fig. 1(a).

3. SPARSE MODEL

We search for the target on a uniform 3D grid inside the breast, as shown in Fig. 1(b). Assuming that there is a target at each node, we derive an approximate linear model

$$\mathbf{e}_i = \mathbf{G}_i \mathbf{c}, \quad (16)$$

$$\mathbf{e}_i = [V(\mathbf{r}_1, \mathbf{r}_i) \quad \dots \quad V(\mathbf{r}_M, \mathbf{r}_i)]_{M \times 1}^T, \quad (17)$$

$$\mathbf{G}_i = \begin{bmatrix} G_{11}(\mathbf{r}_1, \mathbf{t}_i; \mathbf{r}_i) & \dots & G_{1N}(\mathbf{r}_1, \mathbf{t}_N; \mathbf{r}_i) \\ \vdots & \ddots & \vdots \\ G_{M1}(\mathbf{r}_M, \mathbf{t}_1; \mathbf{r}_i) & \dots & G_{MN}(\mathbf{r}_M, \mathbf{t}_N; \mathbf{r}_i) \end{bmatrix}_{M \times N}, \quad (18)$$

$$\mathbf{c} = [c_1 \quad \dots \quad c_N]_{N \times 1}^T, \quad (19)$$

where \mathbf{e}_i is the vector of the received signals when the i th antenna is transmitting, \mathbf{G}_i is the corresponding system matrix, and \mathbf{c} is the unknown vector whose elements are proportional to the permittivity difference, as defined in (7), for each grid node. An element of the system matrix is

$$G_{jk}(\mathbf{r}_j, \mathbf{t}_k; \mathbf{r}_i) = (g_{11}(\mathbf{r}_j, \mathbf{r}_i, \mathbf{t}_k) \cos \alpha_i + g_{12}(\mathbf{r}_j, \mathbf{r}_i, \mathbf{t}_k) \sin \alpha_i) \cos \alpha_j + \\ + (g_{21}(\mathbf{r}_j, \mathbf{r}_i, \mathbf{t}_k) \cos \alpha_i + g_{22}(\mathbf{r}_j, \mathbf{r}_i, \mathbf{t}_k) \sin \alpha_i) \sin \alpha_j, \quad 1 < k < N, \quad 1 < j < M, \quad (20)$$

where \mathbf{t}_k is the position of the k th grid node, N is the size of the grid, and M is the total number of receiving antennas (only i th antenna is transmitting). We combine the measurements related to different transmissions into one set of equations as

$$\mathbf{e} = \mathbf{G}\mathbf{c}, \quad (21)$$

where the stacked measurement vector is

$$\mathbf{e} = \begin{bmatrix} \mathbf{e}_1 \\ \vdots \\ \mathbf{e}_M \end{bmatrix}, \quad (22)$$

and the aggregated system matrix is

$$\mathbf{G} = \begin{bmatrix} \mathbf{G}_1 \\ \vdots \\ \mathbf{G}_M \end{bmatrix}. \quad (23)$$

Under the assumption that the target occupies only a few grid nodes, we apply the l_1 regularization to emphasize the sparsity of the solution vector \mathbf{c} ,

$$\hat{\mathbf{c}} = \min_{\mathbf{c}} \{ \|\mathbf{e} - \mathbf{G}\mathbf{c}\|_2^2 + \lambda \|\mathbf{c}\|_1 \}. \quad (24)$$

Here, $\hat{\mathbf{c}}$ is the estimated coefficient vector and λ is the regularization parameter. To solve (26), we use the CVX package [26], [27]. We compute the regularization parameter, which balances between the data fidelity and the solution sparsity using the L-curve method [28].

We also investigate a different sparse scheme in which the system matrix and the measurement vector are associated with a subset of M transmissions. Namely, we jointly process the data corresponding to a few transmitting antennas. As before, we assume that one transmitter is active at a time. In this case, the measurement vector and the system matrix are obtained from (24) and (25) by keeping \mathbf{e}_i and \mathbf{G}_i , $i = 1, \dots, M$, related to the desired transmitters. The final image is obtained by superimposing partial images (i.e., estimated coefficient vectors) associated with different groups of transmitters.

4. BREST PHANTOM

In our investigations, we used an inhomogeneous breast model (Breast ID: 012204) provided by the UWCEM Numerical Breast Phantom Repository [29], [30]. This repository contains a number of anatomically-realistic breast phantoms derived from the magnetic resonance imaging (MRI). To make the model suitable for the electromagnetic analysis, we decreased its resolution by averaging the electromagnetic parameters of the groups of $10 \times 10 \times 10$ voxels of the original distribution. The resolution of the resulting model was 5 mm and the operating frequency was $f = 1$ GHz. In addition [31], we divided the

obtained continuous range of permittivity (ϵ_r) and conductivity (σ) into 8 domains with the constant parameters defined in Table 1. The relative complex permittivity was defined as $\epsilon = \epsilon_r - j\sigma/(\omega\epsilon_0)$, where the imaginary part of the complex permittivity, $-\sigma/(\omega\epsilon_0)$, takes into account all dielectric losses (polarization and conductive), as in [32]. Besides the true values of the permittivities, Table 1 also shows these values altered for 10%.

Approximately, the domain #1 corresponds to the fatty region, the domains #2–4 belong to the transitional tissue, the domains #5–7 correspond to the fibro-glandular tissue, and the domain #8 is skin. We included the tumor by changing the parameters of one voxel. Its parameters are given in the 9th column of Table 1. Fig. 2 shows the boundaries of the domains, in the order of appearance given in Table 1.

Table 1 Permittivities of homogeneous domains in breast phantom

Domain	1	2	3	4	5	6	7	8	9
ϵ_r	5.5	15	24	32	42	51	60	39	56
ϵ_r (10%)	6.05	16.5	21.60	28.8	46.2	56.1	66.0	39	56
σ [S/m]	0.06	0.21	0.36	0.49	0.68	0.93	1.28	0.9	1

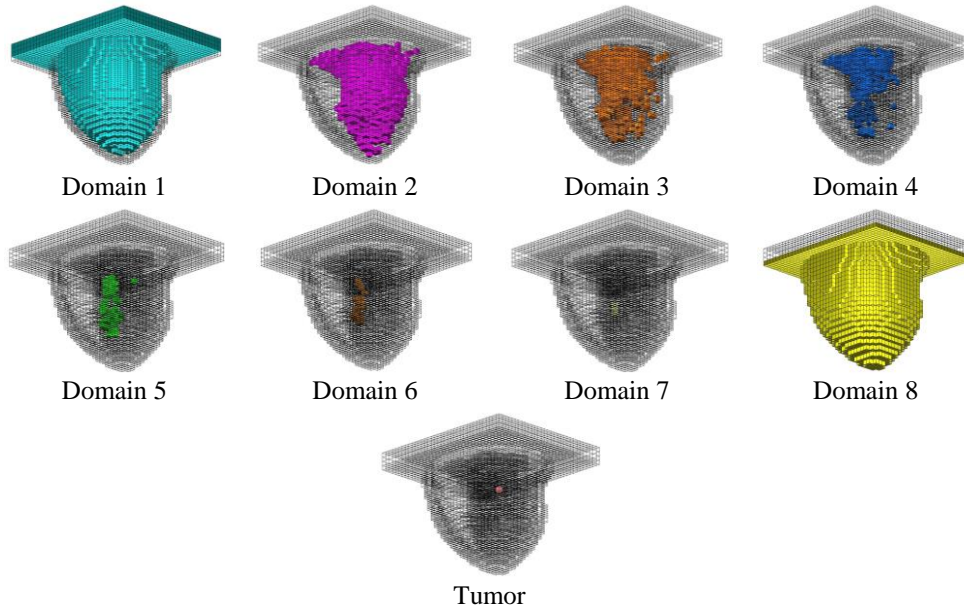


Fig. 2 Different tissues (domains) defined in Table 1

5. NUMERICAL RESULTS

In our numerical simulations, we used an array of $M = 60$ horizontal (quasi-TE polarized) dipoles placed around the breast surface. As illustrated in Fig. 3(a), the dipoles were uniformly distributed along three circular contours. The radii of the contours were 7.8 cm, 8 cm, and

8.3 cm. The corresponding distances of the centers of the contours from the nipple region, along the x -axes, were 5.8 cm, 8.3 cm, and 11.3 cm, respectively. The operating frequency was $f = 1$ GHz. The length of the dipoles was $2h = 2$ cm.

To compute the response of the array and the 3D Green's functions, we used the software WIPL-D Pro [33]. We supposed that the induced signal in the j th antenna, when the i th antenna is transmitting, is proportional to the mutual impedance between those two antennas, i.e., $V(\mathbf{r}_i, \mathbf{r}_j) \approx z_{ij}$. By adding white Gaussian noise, we corrupted the measurement vector. In Fig. 3(b), red lines denote the search space consisting of $N_x = 6$ horizontal cuts. In each cut, the number of the grid nodes was $N_y \times N_z$, $N_y = 32$, $N_z = 32$. The corresponding steps along the coordinate axes were $\Delta_x \approx 9$ mm and $\Delta_y \approx \Delta_z \approx 4.5$ mm. The blue lines in Fig. 3(b) indicate the antenna positions.

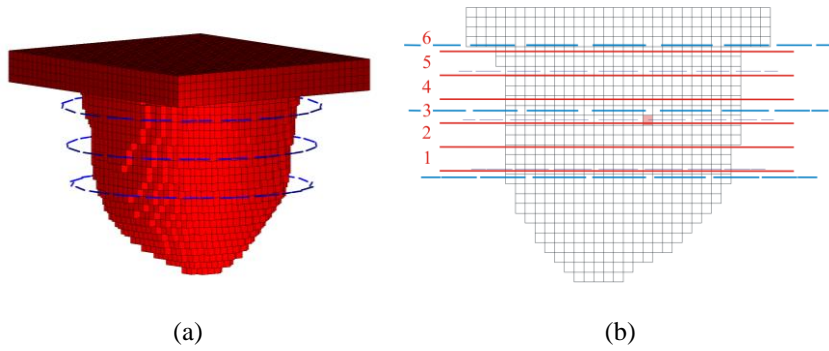


Fig. 3 (a) Antenna array and (b) search space represented by red lines (numbers indicate different cuts)

5.1. Ideal case

First, we considered the case in which we have a perfect knowledge of the breast tissue. We assumed that all $M = 60$ antennas were receiving and every fourth antenna was transmitting (one at a time). Fig. 4 shows the localization result in the cut #3, which was the closest to the target. We simultaneously processed all 6 cuts, as defined in Fig. 3(b). The adopted signal-to-noise ratio was $SNR = 10$ dB. The true position of the scatterer was denoted by a red square marker. The elements of the solution vector in all other planes were zero. The regularization coefficient corresponded to the knee of the L-curve.

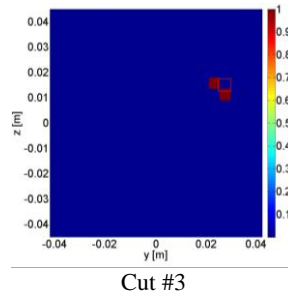


Fig. 4 Ideal case: target image computed for $SNR = 10$ dB

5.2. Incomplete knowledge of dielectric properties

We investigated the robustness of the algorithm against the ambiguity in the breast tissue parameters. In Table 1, we show the permittivity values altered with respect to their adopted values for about 10 %. The experimental setup was the same as in the ideal case. The adopted SNR was 10 dB.

Instead of considering all available data simultaneously, we jointly processed the measured signals associated with groups of adjacent transmitters. Again, we assumed that one transmitter was active at a time. In Fig. 5(a), we give an example of such a group consisting of 4×2 transmitters. The receiving array comprised all antennas. Hence, the corresponding system matrix, as defined by (23), consisted of $Mn_h n_v \times N$ elements, where n_h refers to the number of the transmitters in the horizontal direction and n_v refers to the number of the transmitters in the vertical direction. We shifted the position of the transmitting array for about $kn_h/2$ elements in the horizontal direction and $ln_v/2$ elements in the vertical direction, where $k, l = 0, 1, \dots$. Fig. 5(b) illustrates the position of the shifted array for $k = l = 1$. We obtained the final image by superimposing the partial results obtained using different positions of the transmitting array.

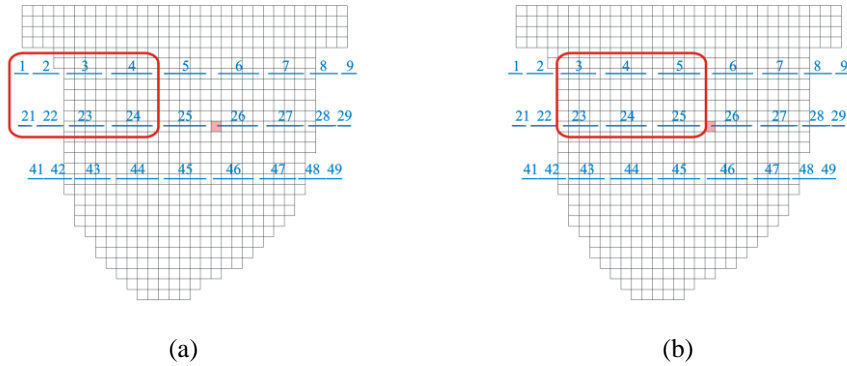


Fig. 5 Example of the transmitting array in (a) its first position and (b) shifted position

Fig. 6 and Fig. 7 show the imaging result for $n_h = 4$ and $n_v = 2$; and for $n_h = 5$ and $n_v = 2$, respectively. In both cases, the location of the tumor was correct in the yz plane (horizontal). In the direction of x -axis, there was an error of about 1 cm. The results in other cuts are several orders of magnitude smaller and they are caused by tissue ambiguity (i.e., false targets).

Numerical investigations showed that the positions of these artifacts varied for different values of n_h . In contrast, the location of the tumor did not change. This dissimilar behavior may be explained by a point-target nature of the tumor as opposed to the distributed nature of the tissue errors.

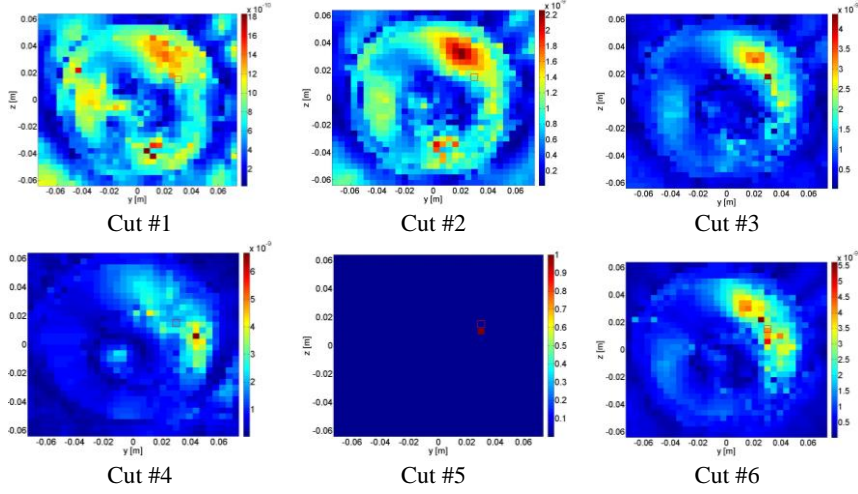


Fig. 6 Sparse imaging results obtained for $n_h = 4$ and $n_v = 2$

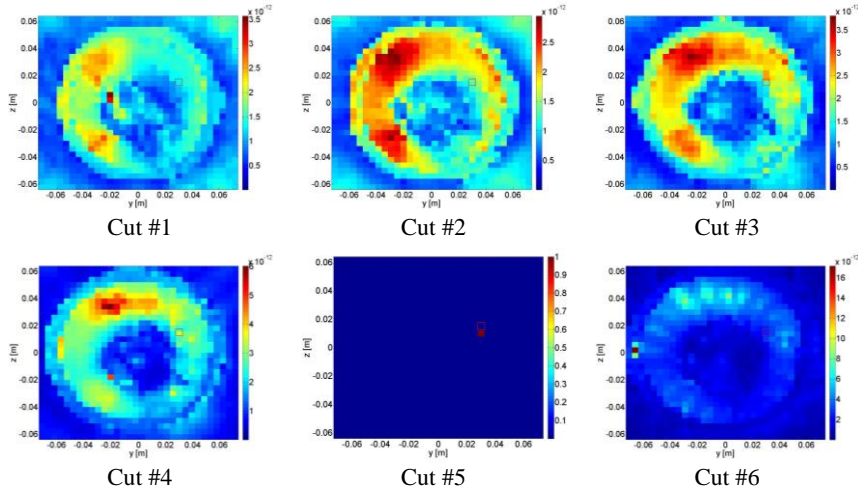


Fig. 7 Sparse imaging results obtained for $n_h = 5$ and $n_v = 2$

6. CONCLUSION

We have proposed a 3D sparsity-based algorithm for differential microwave imaging of tumors inside a known inhomogeneous breast tissue. In contrast to the usual approach available in the literature, we have developed a model in which the trans-polarization due to the inhomogeneous breast tissue was fully taken into account. To check the robustness of the algorithm, we have considered the cases in which the breast tissue was only partially known. To reveal the true position of the tumor and suppress false targets, we applied the sparse processing scheme on different subarrays.

Acknowledgement: *This work was supported by the Serbian Ministry of Science and Education under the Grant TR32005 and by the COST Action TD1301, MiMed.*

REFERENCES

- [1] S. Semenov, "Microwave tomography: Review of the progress towards clinical applications", *Phil. Trans. R. Soc. A*, vol. 367, pp. 3021–3042, 2009.
- [2] A. M. Hassan, M. El-Shenawee, "Review of electromagnetic techniques for breast cancer detection", *IEEE Rev. Biomed. Eng.*, vol. 4, pp. 103–118, 2011.
- [3] P. M. Meaney, M. W. Fanning, T. Raynolds, C. J. Fox, Q. Q. Fang, C. A. Kogel, S. P. Poplack, and K. D. Paulsen, "Initial clinical experience with microwave breast imaging in women with normal mammography", *Acad. Radiol.*, vol. 14, no. 2, pp. 207–218, February 2007.
- [4] S. P. Poplack, K. D. Paulsen, A. Hartov, P. M. Meaney, B. W. Pogue, T. Tosteson, M. Grove, S. Soho, and W. Wells, "Electromagnetic breast imaging-pilot results in women with abnormal mammography", *Radiology*, vol. 243, pp. 350–359, 2007.
- [5] M. Klemm, J. Leendertz, A. W. Preece, M. Shere, I. J. Craddock, and R. Benjamin, "Clinical experience of breast cancer imaging using ultrawideband microwave radar system at Bristol", In Proceedings of the IEEE AP-S Int. Symp., Toronto, ON, Canada, 2010, vol. 501.10.
- [6] P. M. Meaney, D. Goodwin, A. H. Golnabi, T. Zhou, M. Pallone, S. D. Geimer, G. Bruke, and K. D. Paulsen, "Clinical microwave tomographic imaging of the calcaneus: A first-in-human case study of two subjects", *IEEE Trans. Biomed. Eng.*, vol. 59, no. 12, pp. 3304–3313, December 2012.
- [7] I. S. Karanasiou, N. K. Uzunoglu, and C. C. Papageorgiou, "Towards functional noninvasive imaging of excitable tissues inside the human body using focused microwave radiometry", *IEEE Trans. Microw. Theory Techn.*, vol. 52, no. 8, pp. 1898–1908, August 2004.
- [8] A. Fhager and M. Persson, "A microwave measurement system for stroke detection", In Proceedings of the Antennas and Propagation Conference (LAPC), Loughborough, UK, 2011. pp. 14–15.
- [9] R. Scapatucci, L. Di Donato, I. Catapano, and L. Crocco, "A feasibility study on microwave imaging for brain stroke monitoring", *Progress In Electromagnetics Research B*, vol. 40, pp. 305–324, 2012.
- [10] C. Gilmore, A. Abubakar, W. Hu, T.M. Habashy, and P. M. van den Berg, "Microwave biomedical data inversion using the finite-difference contrast source inversion method", *IEEE Trans. Antennas Propag.*, vol. 57, no. 5, pp. 1528–1538, May 2009.
- [11] T. U. Gürbüz, B. Aslanyürek, A. Yapar, H. Şahintürk, I. Akduman, "A nonlinear microwave breast cancer imaging approach through realistic body–breast modeling", *IEEE Trans. Antennas Propag.*, vol. 62, no. 5, pp. 2596–2605, May 2014.
- [12] R. Scapatucci, I. Catapano, and L. Crocco, "Wavelet-based adaptive multiresolution inversion for quantitative microwave imaging of breast tissues", *IEEE Trans. Antennas Propag.*, vol. 60, no. 8, pp. 3717–3726, August 2012.
- [13] J. D. Shea, P. Kosmas, S. C. Hagness, and B. D. Van Veen, "Three-dimensional microwave imaging of realistic numerical breast phantoms via a multiple-frequency inverse scattering technique", *Med. Phys.*, vol. 37, no. 8, pp. 4210–4226, August 2010.
- [14] F. Gao, B. Van Veen, and S. C. Hagness, "Contrast enhanced microwave imaging of breast tumors using sparsity regularization", In Proceedings of the IEEE Antennas Propag. Soc. Int. Symp. (APS-URSI), Chicago, IL, 2012, pp. 8–14.
- [15] D. Winters, B. Van Veen, and S. C. Hagness, "A sparsity regularization approach to the electromagnetic inverse scattering problem", *IEEE Trans. Antennas Propag.*, vol. 58, no. 1, pp. 145–154, January 2012.
- [16] M. Nikolic Stevanovic, L. Crocco, A. Djordjevic, and A. Nehorai, "Higher order sparse microwave imaging of PEC scatterers", *IEEE Trans. Antennas Propag.*, vol. 64, no. 3, March 2016.
- [17] M. Azghani, P. Kosmas, F. Marvasti, "Microwave medical imaging based on sparsity and an iterative method with adaptive thresholding", *IEEE Trans. Med. Imag.*, vol. 34, no. 2, pp. 357–365, February 2015.
- [18] M. Bevacqua, R. Scapatucci, "A compressive sensing approach for 3D breast cancer microwave imaging with magnetic nanoparticles as contrast agent", *IEEE Trans. Med. Imag.*, vol. 35, no. 2, pp. 665–673, February 2016.

- [19] M. Nikolic, J. Dinkic, N. Milosevic, and B. Kolundzija, "Sparse localization of tumors inside an inhomogeneous breast", In Proceedings of the International Conference on Electromagnetics in Advanced Applications (ICEAA), Torino, IT, 2015, pp. 1056–1059.
- [20] D. M. Malioutov, M. Cetin, and A. S. Willsky, "Sparse signal reconstruction perspective for source localization with sensor arrays", *IEEE Trans. Signal Process.*, vol. 53, no. 8, pp. 3010–3022, 2005.
- [21] L. C. Potter, E. Ertin, J.T. Parker, M. Cetin, "Sparsity and compressed sensing in radar imaging", In Proceedings of the IEEE, vol. 98, no. 6, pp. 1006–1020, June 2010.
- [22] E. Porter, G. Walls, Y. Zhou, M. Popović, and J. D. Schwartz, "A flexible broadband antenna and transmission line network for a wearable microwave breast cancer detection system", *Prog. Electromagn. Res. Lett.*, vol. 49, pp. 111–118, 2014.
- [23] E. Porter, M. Coates and M. Popović, "An early clinical study of time-domain microwave radar for breast health monitoring", *IEEE Trans. Biomed. Eng.*, vol. 63, no. 3, pp. 530–539, March 2016.
- [24] R. Scapatucci, O. M. Bucci, I. Catapano, and L. Crocco, "Differential Microwave Imaging for Brain Stroke Followup", *Int. J. Antennas Propag.*, vol. 2014, Article ID 312528, 11 pages, 2014.
- [25] W.C. Chew, *Waves and fields in inhomogenous media*, Wiley-IEEE Press, February 1999.
- [26] M. Grant and S. Boyd, CVX: Matlab software for disciplined convex programming, <http://stanford.edu/~boyd/cvx>, June 2009.
- [27] M. Grant and S. Boyd, Graph implementations for non smooth convex programs, Recent advances in learning and control (a tribute to M. Vidyasagar), V. Blondel, S. Boyd, and H. Kimura, editors, *Lecture Notes in Control and Information Sciences*, Springer, 2008, pp. 95-110.
- [28] P. C. Hansen and D. P. O'Leary, "The use of the L-curve in the regularization of discrete ill-posed problems", *SIAM J. Sci. Comput.*, vol. 14, no. 6, pp. 1487–1503, 1993.
- [29] E. Zastrow, S. K. Davis, M. Lazebnik, F. Kelcz, B. D. Van Veen, S. C. Hagness, Database of 3D grid-based numerical breast phantoms for use in computational electromagnetics simulations.
- [30] M. Lazebnik, L. McCartney, D. Popovic, C. B. Watkins, M. J. Lindstrom, J. Harter, S. Sewall, A. Magliocco, J. H. Booske, M. Okoniewski, and S. C. Hagness, "A large-scale study of the ultrawideband microwave dielectric properties of normal breast tissue obtained from reduction surgeries", *Phys. Med. Biol.*, vol. 52, pp. 2637–2656, April 2007.
- [31] N. Milosevic, M. Nikolic, B. Kolundzija, J. Music, "Numerical heterogeneous breast phantoms with different resolutions", In Proceedings of the EUCAP, Lisbon, PT, 2015.
- [32] A. Djordjević, D. Olčan, M. Stojilović, M. Pavlović, B. Kolundžija, D. Tošić, "Causal models of electrically large and lossy dielectric bodies", *Facta Universitatis, Series: Electronics and Energetics*, vol. 27, no. 2, pp. 221–234, June 2014.
- [33] <http://www.wipl-d.com/>